



# (p,2p) Reactions on $^{9-16}\text{C}$ at 250 MeV/A

T. Kobayashi <sup>a,\*</sup> K. Ozeki <sup>b</sup> K. Watanabe <sup>a</sup> Y. Matsuda <sup>a</sup> Y. Seki <sup>a</sup>  
T. Shinohara <sup>a</sup> T. Miki <sup>a</sup> Y. Naoi <sup>a</sup> H. Otsu <sup>a,1</sup> S. Ishimoto <sup>c</sup> S. Suzuki <sup>c</sup>  
Y. Takahashi <sup>d</sup> E. Takada <sup>e</sup>

<sup>a</sup> *Department of Physics, Graduate School of Science, Tohoku University, 2-1 Aoba. Aramaki, Aoba, Sendai 980-8578, Japan*

<sup>b</sup> *CYRIC, Tohoku University, 2-1 Aoba. Aramaki, Aoba, Sendai 980-8578, Japan*

<sup>c</sup> *KEK, 1-1 Oho, Tsukuba, Ibaraki 305-0801, Japan*

<sup>d</sup> *RCNP, Osaka University, 10-1 Mihogaoka, Ibaraki, Osaka 567-0047, Japan*

<sup>e</sup> *NIRS, 4-9-1 Anagawa, Inage, Chiba, Chiba 263-8555, Japan*

---

## Abstract

Proton knockout reactions on carbon isotopes  $p(^{9-16}\text{C},2p)^{8-15}\text{B}$  at 250 MeV/A were performed for systematic information on weakly- to strongly-bound 1p valence protons and deeply-bound 1s inner-shell protons. Various information such as the s-hole distributions, excitation energy of the s-hole states, momentum widths for 1s and 1p orbits, and relative (p,2p) yields are obtained.

*Key words:* Proton knockout reaction,

*PACS:* 25.60.Gc, 27.20+n

---

## 1. Introduction

Proton knockout (p,2p) reactions are among the most direct experimental techniques to study single-particle properties of nuclei such as the separation energy, momentum distributions, angular momenta, and spectroscopic factors, of bound protons in the nucleus, as demonstrated for stable nuclei using high-energy proton beams [1,2]. The bound proton in the target nucleus is knocked out via quasifree proton-proton scattering, and a hole state is produced as a residual nucleus. By measuring 4-momenta of two protons

---

\* Corresponding author.

*Email address:* [kobayash@lambda.phys.tohoku.ac.jp](mailto:kobayash@lambda.phys.tohoku.ac.jp) (T. Kobayashi).

<sup>1</sup> Present address: RIKEN, 2-1 Hirosawa, Wako, Saitama 351-0198, Japan

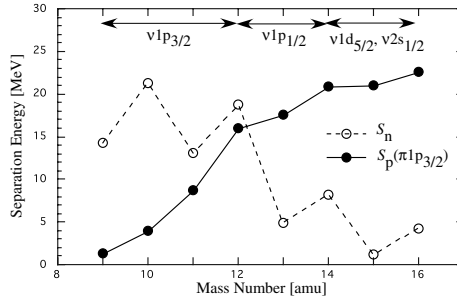


Fig. 1. Neutron separation energy  $S_n$  (open circle) and proton separation energy  $S_p$  (closed circle) for  ${}^9\text{--}{}^{16}\text{C}$ .

in the final state, the separation energy  $S_p$  and momentum  $\vec{q}$  of the knocked out proton are obtained. This method can be used to study the single-particle properties of both valence and inner-shell orbits because a nucleon is used as a probe. The application of this method to unstable nuclei with radioactive (RI) beams on a proton target is very promising.

Nucleon knockout reactions from RI beams using nuclear targets such as Be, where the excited states are tagged by  $\gamma$ -rays, have been extensively studied at MSU and GSI [3]. Momentum distributions of the heavy residue after the knockout reaction are measured for identifying the angular momentum and spectroscopic factors are deduced. These experiments were restricted mainly to valence-neutron knockout to ground and particle-stable excited states induced by the nuclear target.

We present here the first systematic studies of the (p,2p) proton-knockout reactions in the inverse kinematics on eight carbon isotopes ranging from  ${}^9\text{C}$  to  ${}^{16}\text{C}$ . The neutron separation energy  $S_n$  of the valence orbit decreases from 20 MeV down to 1 MeV with a zigzag pattern with increasing neutron numbers. The proton separation energy  $S_p$  of the valence  $\pi 1p_{3/2}$  orbit, on the other hand, increases from 1.3 MeV for  ${}^9\text{C}$  to 16.0 MeV for  ${}^{12}\text{C}$ , and increases further up to 22.6 MeV for  ${}^{16}\text{C}$ , as shown in Fig. 1. The proton separation energy of the inner-shell ( $\pi 1s_{1/2}$ ) orbit is about 20 MeV larger. Therefore, the (p,2p) proton knockout reaction on carbon isotopes provides a chance to study the variation of weakly to strongly-bound valence  $\pi 1p_{3/2}$  orbit, and also very strongly (30 to 50 MeV)-bound inner-shell  $\pi 1s_{1/2}$  orbit as neutrons are added to the nucleus.

For the (p,2p) knockout reaction to be quasifree, the beam energy of the RI beams needs to be relatively high. Restricted both by the maximum energy of the secondary beam line and the capability for the total-energy measurement of high-energy protons, beam energy was chosen at about 250 A MeV. The measurement in the inverse kinematics, i.e. RI beams on the proton target, provides additional useful information. Since the hole state is produced with the beam velocity into a narrow cone in the forward direction, the decay modes of the hole state can be measured simultaneously with high efficiency by detecting the hole state itself or particles from the decay of the hole states in the forward direction.

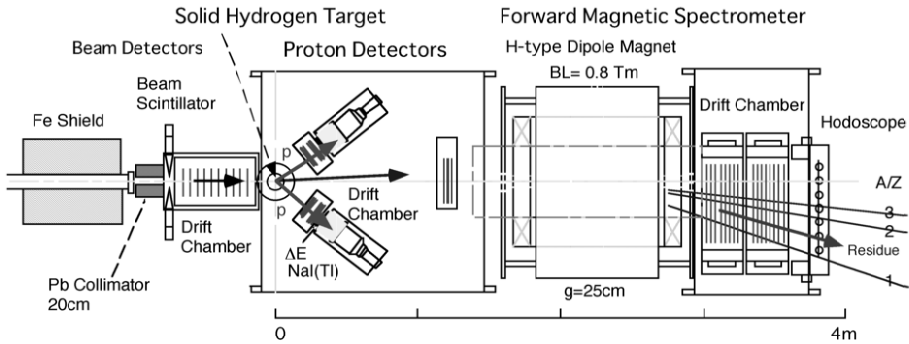


Fig. 2. Experimental setup

## 2. Experiment

The experiment was performed at the HIMAC (Heavy Ion Medical Accelerator in Chiba) accelerator facility in NIRS (National Institute of Radiological Sciences). Primary  $^{12}\text{C}$  and  $^{18}\text{O}$  beams were accelerated to 350–400 MeV/A by the heavy-ion synchrotron with a typical intensity of  $3 \times 10^9$  particles/spill, and 10–15 g/cm<sup>2</sup>-thick Be target was used as a production target. Carbon isotope beams of  $^{9-16}\text{C}$  at 250 AMeV with a momentum spread of  $\pm(0.1-2.5)\%$  were separated and momentum tagged by the secondary beam line SB2, and focused onto a reaction target at F3. Secondary beam intensities were  $10^4$  to  $10^5$  particles/spill, depending on the isotope. The experimental setup at F3 is shown in Fig. 2.

The secondary beam passed through 2 mm-thick plastic scintillators for energy-loss and time-of-flight measurements, and the direction of the beam particles was measured by the beam drift chamber.

The solid-hydrogen target (SHT) was mounted in a vacuum chamber with 50  $\mu\text{m}$ -thick Kapton foils as entrance and exit windows. The thickness and diameter of the SHT was 5 mm (44 mg/cm<sup>2</sup>) and 30 mm respectively. Two 9  $\mu\text{m}$ -thick Mylar foils separated the SHT from the vacuum. The SHT was essential to avoid the background and to reduce the multiple Coulomb scattering. Typical S/N ratio with and without was more than 100.

Two protons from the (p,2p) reaction were detected by two proton telescopes set at  $\pm 39^\circ$  with an angular acceptance of  $\pm 9^\circ$  in both horizontal and vertical directions. The geometry is optimized to detect two protons from the quasifree p-p scattering around  $90^\circ$  in the p-p center of mass. The proton telescope consists of 5 mm-thick plastic scintillator for energy-loss, the drift chamber for tracking, and 6"  $\phi \times 5$ "-thick NaI(Tl) for the total-energy measurement. Protons between 20 to 210 MeV can be measured and identified. The proton energies were calibrated by p(p,2p) reactions using 210 MeV proton beams.

The forward magnetic spectrometer was used to detect and identify forward particles produced in the (p,2p) reaction. It consists of H-type dipole magnet with 25 cm gap, 3 sets of drift chambers for tracking, and plastic scintillator hodoscope for energy-loss and time-of-flight. By combining magnetic analysis, charge, and TOF measurements, the mass resolution  $\sigma_A$  was about 0.25 amu.

### 3. Analysis and Results

Proton separation energy  $S_p$  and momentum  $\vec{q}$  of knocked out proton in the projectile are calculated from 4-momenta of two protons.

#### 3.1. Separation Energy Distribution

Proton separation energy distributions are shown in Fig. 3. Distributions in Fig. 3A are obtained by only using information of two protons. Distributions consist of sharp peaks corresponding to the p-hole states and broad bumps corresponding to the s-hole states. The separation-energy distribution for  $^{12}\text{C}$  is consistent with that obtained by the  $^{12}\text{C}(\text{p},2\text{p})$  reaction using 400 MeV proton beams [4].

We further required two additional conditions to select the transition to the ground state via the  $^A\text{C}(\text{p},2\text{p})^{A-1}\text{B}_{gr}$  reaction and also to select the transition to the s-hole states.

Distributions in Fig. 3B are obtained by requiring the detection of mass-identified boron isotopes  $^{A-1}\text{B}$  in the forward spectrometer. Since  $^9\text{B}$  produced in the  $^{10}\text{C}(\text{p},2\text{p})$  reaction is particle unstable, treatment is slightly different. The major part of the distribution is via the direct transition to the ground state, and also a small amount of transitions to particle-stable excited states are seen. Direct transition to the ground state can be selected by additionally setting appropriate energy gates on these distributions around the ground state. From the widths of the distributions, the separation-energy resolution in the present measurement was  $\sigma(S_p) \sim 1.3$  MeV, limited mainly by the angular resolution of the proton telescope. The ambiguity in the offset energy was about 0.3 MeV.

Since the s-hole states are produced with high excitation energy, charged particles are expected to be emitted from the decay of the s-hole states. In order to select this condition, we require that there are no boron isotopes detected in the forward magnetic spectrometer, as shown in Fig. 3C. Further energy gates are set above the proton-emission threshold on these distributions to select the s-hole states.

As shown in Fig. 3C, the s-hole states in the carbon isotopes are systematically observed. Since the observed distribution is distorted by the finite geometrical acceptance of the detector system, simulation was performed to correct for the acceptance. In the simulation, two assumptions were made: the p-p angular distribution is isotropic in the p-p center of mass, and the momentum distribution is a harmonic oscillator. The simulation shows that the acceptance has a broad maximum at  $S_p \sim 30$  MeV. After correcting for the acceptance, the s-hole distributions are fitted by the functional form, and the peak value and the width of the s-hole states are obtained. The excitation energy of the s-hole states relative to the boron ground state is shown in Fig. 4. It has a broad minimum at  $A \sim 12$ . The attractive force [5] between  $\nu 1p_{1/2}$  and  $\pi 1p_{3/2}$  may explain the increase in the neutron-rich side. Since the identification of the s-hole states in  $^9\text{C}$  has some ambiguities, data for  $^9\text{C}$  is tentative.

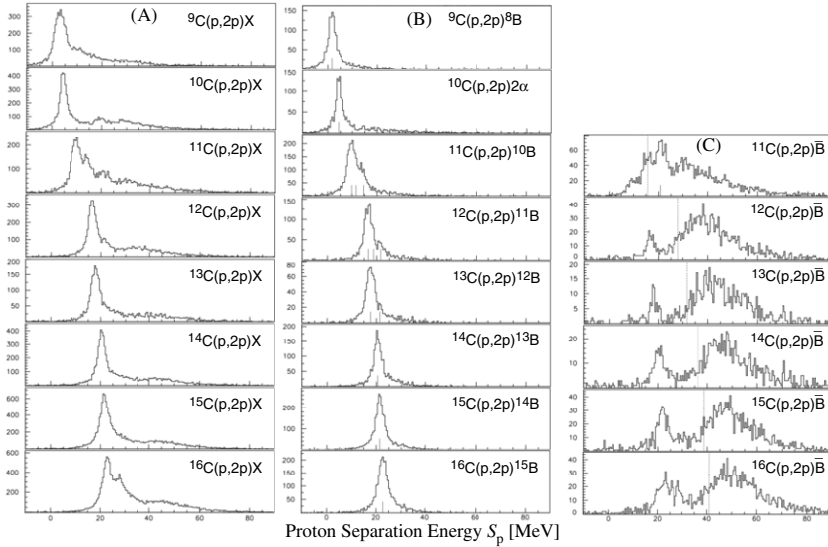


Fig. 3. Proton-separation-energy distributions: (A) inclusive, (B)  $A-1B$  detected in the forward spectrometer, (C) no boron isotopes detected (labeled as  $\bar{B}$ ) in the forward spectrometer

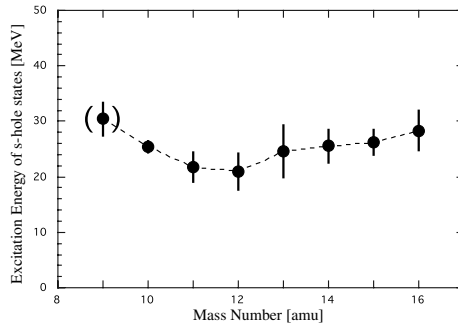


Fig. 4. Excitation energy of the s-hole states relative to the boron ground state. Data for  $^9C$  is tentative.

### 3.2. Momentum Distribution

Momentum distributions of protons in 1s and 1p orbit are obtained by setting appropriate energy gates on the  $S_p$  distribution as shown in Fig. 3C and Fig. 3B, respectively. Effect of the finite geometrical acceptance is corrected for by the simulation. The assumption of isotropic pp scattering is also made. For example, the acceptance drops down by  $\sim 50\%$  at  $q=200$  MeV/c for the 1p orbit at  $S_p=16$  MeV. The momentum distributions  $\frac{dN}{dq}$  for the p-hole states via the  $^A C(p,2p)^{A-1}B_{gr}$  reaction and for the s-hole states via the  $^A C(p,2p)\bar{B}$  reaction are shown in Fig. 5. These distributions are fitted by the harmonic oscillator wave functions  $\frac{dN}{dq} \propto q^{2\ell+2} \exp(-q^2/\sigma_\ell^2)$  in order to get the momentum widths  $\sigma_0$  for  $\ell=0$  (1s) and  $\sigma_1$  for  $\ell=1$  (1p).

Angular momentum  $\ell$  can be uniquely identified, except few cases, by comparing the reduced  $\chi^2$  of the fitting. The widths are summarized in Fig. 6A. The widths of the p hole states via  $^A C(p,2p)^{A-1}B_{IAS}$  reactions for  $^9C$  and  $^{10}C$  are also shown. The momentum

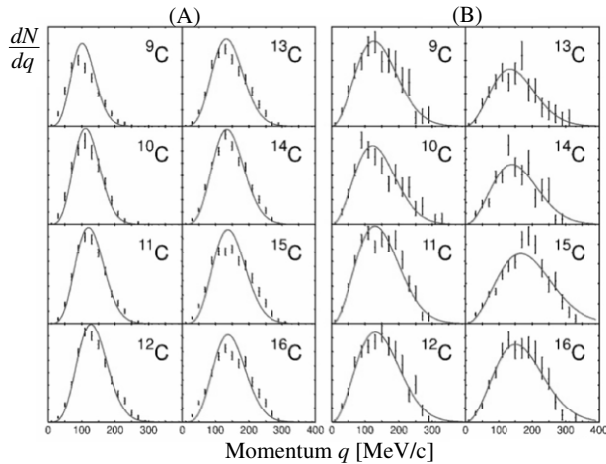


Fig. 5. Proton Momentum distributions  $\frac{dN}{dq}$ . (A) for the p-hole states via  ${}^A\text{C}(p,2p){}^{A-1}\text{B}_{gr}$  reaction. (B) for the s-hole states via  ${}^A\text{C}(p,2p){}^{A-1}\text{B}_{s}$  reaction.

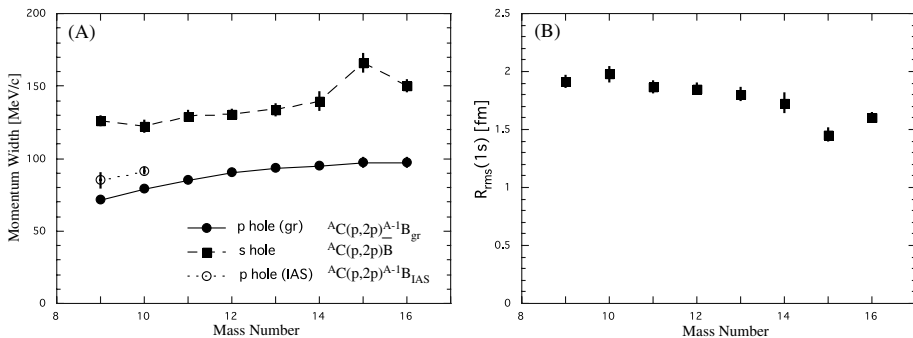


Fig. 6. (A) Momentum widths of harmonic oscillator wave function,  $\sigma_0$  for the 1s orbit (closed square) and  $\sigma_1$  for the 1p orbit (closed circle). (B) Rms charge radii of the 1s orbit.

widths for  ${}^{12}\text{C}$  are consistent with those obtained by the  ${}^{12}\text{C}(e,e'p)$  reaction [6].

The momentum width of the p orbit increases monotonically from proton-rich to neutron-rich side, reflecting the weak binding nature of valence protons in the proton-rich side. Momentum width of the s orbit is also gradually increasing toward the neutron-rich side. Simple potential model after adjusting the proton separation energy qualitatively reproduces the general tendency. On the other hand, the same model gives rather constant momentum width, independent of the separation energy for the s orbit.

From the momentum widths of the s orbit, root mean square charge radii of the 1s orbit can be deduced assuming the harmonic oscillator wave function. The charge radii decreases from 2.0 fm in the proton-rich side down to 1.5 fm in the neutron-rich side as shown in Fig. 6B. The present observation indicates that the proton radii of the core is gradually shrinking toward the neutron-rich side. A similar phenomenon was observed by the laser spectroscopy showing that the charge radii of  ${}^{6,7,8,9}\text{Li}$  decrease gradually toward the neutron-rich side [7].

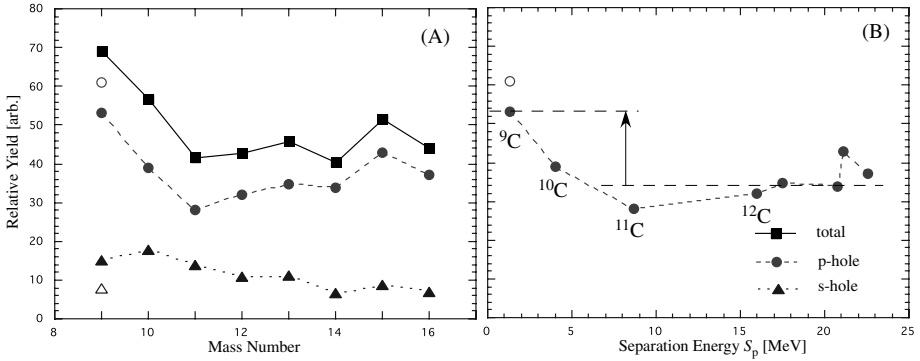


Fig. 7. Relative (p,2p) yield as a function of the mass number (A) and the separation energy (B). Closed square, closed circle, closed triangle are for total, p-hole, and s-hole states, respectively.

### 3.3. Relative (p,2p) Yields

Relative (p,2p) yields for the p-hole and s-hole states are obtained after the acceptance correction. The p-hole states were identified by requiring boron isotopes in the forward spectrometer, while the s-hole states were identified by requiring no boron isotopes in the forward spectrometer. The results are summarized in Fig. 7. Total yield is rather constant between  $^{11}\text{C}$  and  $^{16}\text{C}$ , and the yield is about 50% larger for  $^9\text{C}$ . Since there are some ambiguities for the assignment of the s- and p-hole states in  $^9\text{C}$ , two possibilities are shown by closed and open symbols. When yields are divided into the p-hole and s-hole components, it is the p-hole component, which is increasing at  $^9\text{C}$ . Since the relative yield is expected to be proportional to the spectroscopic factor, the present observation also indicates that the spectroscopic factor for the weakly-bound valence proton is larger, as in the case of the knockout reactions [3]. There is also a tendency that the yield for the s-hole states is decreasing toward the neutron-rich side. Since very-strongly bound s orbit is involved, it is not clear whether the reason for the reduction is due to the variation of the spectroscopic factor of deeply-bound core protons or due to the reaction mechanism.

## 4. Summary

Proton knockout (p,2p) reactions from  $^9\text{--}^{16}\text{C}$  isotopes at 250 MeV/A were performed for systematic information on weakly- to strongly-bound 1p valence protons and deeply-bound 1s inner-shell protons. Separation energy distributions are measured with about 1.3 MeV (rms) resolution. The s-hole and p-hole states are identified and separated by tagging the decay mode of the hole states. The excitation energy of the s-hole states has a shallow minimum around  $^{12}\text{C}$ . Momentum widths of the 1p valence orbit are narrower toward proton-rich side reflecting the weak binding nature of valence protons in the proton-rich side. The momentum widths of the 1s core orbit show increase toward the neutron-rich side, indicating that the charge radii of the 1s orbit are shrinking towards the neutron-rich side. The relative (p,2p) yields indicate that the weakly-bound valence proton in  $^9\text{C}$  have larger spectroscopic factors compared other carbon isotopes.

## Acknowledgment

The experiment was supported by the Research Project with Heavy Ions at NIRS-HIMAC.

## References

- [1] Gerhard Jacob and Th.A.J. Maris, *Rev. Mod. Phys.* **38**, (1966) 121.
- [2] Gerhard Jacob and TH.A.J. Maris, *Rev. Mod. Phys.* **45**, (1973) 6.
- [3] P.G. Hansen and J.A. Tostevin, *Annu. Rev. Nucl. Sci.* **53**, (2003) 219.
- [4] M. Yosoi et al., *Phys. Lett.* **B551**, (2003) 255 .
- [5] T. Otsuka et al., *Phys. Rev. Lett.* **87**, (2001) 082502 .
- [6] J. Mougey et al., *Nucl. Phys.* **A262**, (1976) 462.
- [7] G. Ewald et al., *Phys. Rev. Lett.* **93** (2004) 113002.